# Cation Ordering and Electrochemical Properties of the Cathode Materials $LiZn_xMn_{2-x}O_4$, $0 < x \leq 0.5$: A $^6Li$ Magic-Angle Spinning NMR Spectroscopy and Diffraction Study

Young Joo Lee,[†] So-Hyun Park,[‡] Charlotte Eng,[†] John B. Parise,[†,‡] and Clare P. Grey*[,†]

*Department of Chemistry, State University of New York at Stony Brook, Stony Brook, New York 11794-3400, and Department of Geosciences, State University of New York at Stony Brook, Stony Brook, New York 11790-2100*

*Received May 21, 2001. Revised Manuscript Received September 21, 2001*

The local and long-range structures of $LiZn_xMn_{2-x}O_4$ ($x = 0.1$, 0.2, 0.3, 0.5) have been studied by using $^6Li$ magic-angle spinning (MAS) NMR spectroscopy and X-ray and neutron powder diffraction. For all the samples, a $^6Li$ resonance at approximately 2000 ppm is observed due to the presence of Li in the octahedral sites of the spinel structure, indicating that Zn substitutes for lithium in the tetrahedral sites. For low doping levels ($x = 0.1$ and 0.2), several resonances at 500−700 ppm are seen, which are assigned to lithium cations in tetrahedral sites with local environments such as $Li(OMn^{3.5+})_{12-y}(OMn^{4+})_y$, $Mn^{3.5+}$ indicating a Mn ion with an average oxidation state of 3.5. The $x = 0.3$ sample is not obtained as a single phase; instead, two phases with Zn-doping levels corresponding to $x = 0.2$ and 0.5 are observed. Different cation-ordering schemes are observed for the $x = 0.5$ sample, depending on the condition of synthesis: slow cooling from 700 °C to room temperature results in cation ordering in both tetrahedral and octahedral sites, whereas the sample quenched from high temperature shows no long-range cation ordering on either site. The structure of ordered $Li_{0.5}Zn_{0.5}[Mn_{1.5}Li_{0.5}]O_4$ was refined by using neutron and X-ray powder diffraction data in the space group $P2_13$ and shows complete ordering on the octahedral site but some partial disorder or cation vacancies on the tetrahedral site. The variable temperature $^6Li$ NMR spectra are consistent with a gradual change in the nature of the magnetic interactions between the manganese spins, from antiferromagnetic (for the sample with the lowest Zn-doping level) to ferromagnetic (for ordered $Li_{0.5}Zn_{0.5}[Mn_{1.5}Li_{0.5}]O_4$), as the concentration of Zn increases. The $^6Li$ NMR spectra of $LiZn_{0.1}Mn_{1.9}O_4$ during the first charging cycle shows a gradual shift in the peak position to higher frequency, rather than a series of discrete resonances. This is consistent with the potential vs charging profiles, where the two potential plateaus that are typically seen in the charging/discharging potential profiles of $LiMn_2O_4$ are no longer observed. Li ions remain in the octahedral site throughout.

## Introduction

The increasingly widespread use of portable electronic technology has created a high demand for rechargeable batteries that are lightweight but have high energy densities and long cycle lives. Considerable attention has been focused on host materials that contain Co, Ni, and Mn and can reversibly intercalate lithium ions.[1,2] The first commercial and the most effective rechargeable battery to date is the cell containing a $LiCoO_2$ cathode and a carbon anode, with the lithium ions shuttling back and forth between two intercalation hosts producing a 4 V output voltage.[3] In comparison to the Co- and Ni-containing cathode materials, lithium manganese oxides represent particularly attractive materials, since they are considerably cheaper and nontoxic. The spinel $Li_xMn_2O_4$ still represents the most promising manganese cathode material developed so far.[4,5] Lithium intercalation occurs at 3 V in the range $1 \leq x \leq 2$ but is associated with a severe capacity loss on repeated cycling. This is ascribed to the large change in volume between the cubic $LiMn_2O_4$ and tetragonal $Li_2Mn_2O_4$ phases (that coexist during charging and discharging), due to the cooperative Jahn−Teller distortion that is observed for the Mn(III) compound.[6] In contrast, $Li_xMn_2O_4$ can perform as a 4 V cell in the range $0 \leq x \leq 1$, retaining a cubic cell throughout and consequently giving better cyclability. It still suffers from a low

* To whom correspondence should be addressed.
[†] Department of Chemistry.
[‡] Department of Geosciences.

(1) Bruce, P. G. *Chem. Commun.* **1997**, 1817.
(2) Thackeray, M. M. *J. Electrochem. Soc.* **1995**, *142*, 2558.
(3) Nagaura, T.; Tozawa, K. *Prog. Batteries Sol. Cells* **1990**, *9*, 209.
(4) David, W. I. F.; Thackeray, M. M.; de-Picciotto, L. A.; Goodenough, J. B. *J. Solid State Chem.* **1987**, *67*, 316.
(5) Thackeray, M. M.; David, W. I. F.; Bruce, P. G.; Goodenough, J. B. *Mater. Res. Bull.* **1983**, *18*, 461.
(6) Le Cras, F.; Anne, M.; Bloch, D.; Strobel, P. *Solid State Ionics* **1998**, *106*, 1.

10.1021/cm010503j CCC: $22.00 
Published on Web 11/22/2001

specific capacity, however, and poor cycling behavior after repeated charging and discharging cycles. Several mechanisms have been suggested for this capacity fade.[7−14] One mechanism involves the Jahn−Teller distortion of $LiMn_2O_4$ in the deeply discharged state, which has been proposed to be a particular problem, even when cycling in the 4 V region, if rapid discharge rates are used. This mechanism can result in structural fatigue and eventually loss in electrical contacts between particles.[13]

One potential approach to combat the Jahn−Teller distortion problem, at the expense of the initial capacity at 4 V, is to increase the manganese oxidation state at the end of discharge by cation doping with appropriate metal ions (e.g., Li, Ni, Cu, Zn, Co, Cr, Al, Mg).[7,15−19] This may also alter the mechanism and numbers of different phases that coexist during charging, affecting the performance of the material over repeated cycling. As the amount of dopant increases, the two-step potential profile becomes less distinctive, consistent with a change in the intercalation/deintercalation process. In a study of the Cr-substituted spinel, the enhanced stability was ascribed to Cr occupancy of the octahedral sites, with the Cr octahedra retaining a regular symmetry, with no Jahn−Teller distortions, throughout the charging and discharging process.[20,21] Some of the metal-doped spinels exhibit additional plateaus at higher potentials (>4.5 V) in the cycling curve, due to the oxidation of the dopant metal. For example, cell voltages of 4.7 V were found for $LiNi_xMn_{2-x}O_4$,[15] 4.9 V for $LiCr_xMn_{2-x}O_4$,[20] and 4.9 V for $LiCu_xMn_{2-x}O_4$.[16]

The dopant cations can substitute at either the octahedral or tetrahedral sites of the spinel structure. Many ternary and quaternary spinels have been studied and the cation distributions, i.e., normal vs inverse spinels, have been identified. Ni cations have been shown to occupy only the octahedral site, whereas Zn, Mg, and Co ions show strong preferences for the tetrahedral sites in the lithium titanate and germanate quaternary spinels $LiM_{0.5}Ti_{1.5}O_4$ and $LiM_{0.5}Ge_{1.5}O_4$, with M = Mg, Co, Ni, Zn.[22,23] These systems also show ordering in the octahedral site, leading to a reduction of the symmetry of the spinel to space group $P4_332$. Lithium manganese oxide spinels with various metal substitutions have been investigated. For example, $Cu^{2+}$ ions substitute in both the octahedral and tetrahedral sites of lithium manganese spinels, forcing some of the lithium cations into the octahedral sites.[16] X-ray diffraction (XRD) studies of $LiMg_{0.5}Mn_{1.5}O_4$ reveal a superstructure due to ordering of the Mn and Mg ions over the octahedral sites.[24−26] In contrast, cation ordering could not be detected by XRD for $LiM_{0.5}Mn_{1.5}O_4$, with M = Co, Ni, and Cu.[24] The ordering of Co and Mn in the octahedral site was proposed on the basis of results from static lattice simulations.[27] Ferrimagnetic behavior was observed for $LiNi_{0.5}Mn_{1.5}O_4$, and this phenomenon was also explained by invoking cation ordering.[28] Our recent $^6$Li NMR results provided direct evidence that cation ordering occurs, the extent of ordering depending on the synthesis conditions.[29] An unusual cation-ordering scheme has been proposed for $LiZn_{0.5}Mn_{1.5}O_4$, where Zn has a preference for the tetrahedral site, forming $(Li_{0.5}Zn_{0.5})_{Td}[Li_{0.5}Mn_{1.5}]_{Oh}O_4$.[26,28,30] Three different structures were proposed in this early work, depending on the history of the heat treatment: a disordered phase with a space group $Fd\bar{3}m$ was seen for the material quenched from 750 °C, a structure with cation ordering in octahedral sites ($P4_332$ space group) was observed for the material quenched from 600 °C, and a structure with cation ordering in both octahedral and tetrahedral sites ($P2_13$ space group) was seen for the slowly cooled material.[26,30] These ordering schemes were proposed based on the indexing of the XRD patterns of the different phases.

Despite considerable work in this field, many details concerning how the dopant metals affect the cycling behavior remain poorly understood. In particular, the effect of different cation distributions on deintercalation mechanisms remains unclear. Lithium NMR represents an ideal method with which to probe the local atomic and electronic structures in these compounds. $^7$Li NMR shows larger quadrupolar interactions and dipolar couplings (between the nuclear and the electronic spins) than does $^6$Li NMR, due to the larger quadrupole moment and gyromagnetic ratio of $^7$Li. Thus, higher resolution magic-angle spinning (MAS) NMR spectra are typically obtained for $^6$Li, often providing more detailed information concerning the local structure. However, the low natural abundance of $^6$Li (6.9%) gives rise to weak NMR signals and represents a problem particularly when studying the delithiated cathodes. This problem can be readily overcome by $^6$Li enrichment, and spectra can be acquired at lower static

(7) Gummow, R. J.; de-Kock, A.; Thackeray, M. M. *Solid State Ionics* **1994**, *69*, 59.
(8) Jang, D. H.; Shin, Y. J.; Oh, S. M. *J. Electrochem. Soc.* **1996**, *143*, 2204.
(9) Amatucci, G. G.; Schmutz, C. N.; Blyr, A.; Sigala, C.; Gozdz, A. S.; Larcher, D.; Tarascon, J. M. *J. Power Sources* **1997**, *69*, 11.
(10) Du-Pasquier, A.; Blyr, A.; Courjal, P.; Larcher, D.; Amatucci, G.; Gérand, B.; Tarascon, J. M. *J. Electrochem. Soc.* **1999**, *146*, 428.
(11) Xia, Y.; Zhou, Y.; Yoshio, M. *J. Electrochem. Soc.* **1997**, *144*, 2593.
(12) Suzuki, K.; Oumi, Y.; Takami, S.; Kubo, M.; Miyamoto, A.; Kikuchi, M.; Yamazaki, N.; Mita, M. *Jpn. J. Appl. Phys.* **2000**, *39*, 4318.
(13) Thackeray, M. M.; Shao-Horn, Y.; Kahaian, A. J.; Kepler, K. D.; Skinner, E.; Vaughey, J. T.; Hackney, S. A. *Electrochem. Solid-State Lett.* **1998**, *1*, 7.
(14) Aurbach, D.; Zaban, A.; Schechter, A.; Ein-Eli, Y.; Zinigrad, E.; Markovsky, B. *J. Electrochem. Soc.* **1995**, *142*, 2873.
(15) Zhong, Q.; Bonakdarpour, A.; Zhang, M.; Gao, Y.; Dahn, J. R. *J. Electrochem. Soc.* **1997**, *144*, 205.
(16) Ein-Eli, Y.; Lu, S. H.; Rzeznik, M. A.; Mukerjee, S.; Yang, X. Q.; McBreen, J. *J. Electrochem. Soc.* **1998**, *145*, 3383.
(17) Song, D.; Ikuta, H.; Uchida, T.; Wakihara, M. *Solid State Ionics* **1999**, *117*, 151.
(18) Robertson, A. D.; Lu, S. H.; Howard, W. F., Jr. *J. Electrochem. Soc.* **1997**, *144*, 3505.
(19) Tarascon, J. M.; Wang, E.; Shokoohi, F. K.; Mckinnon, W. R.; Colson, S. *J. Electrochem. Soc.* **1991**, *138*, 2859.
(20) Sigala, C.; Guyomard, D.; Verbaere, A.; Piffard, Y.; Toumoux, M. *Solid State Ionics* **1995**, *81*, 167.
(21) Ammundsen, B.; Jones, D. J.; Roziere, J.; Villain, F. *J. Phys. Chem. B* **1998**, *102*, 7939.
(22) Kawai, H.; Tabuchi, M.; Nagata, M.; Tukamoto, H.; West, A. R. *J. Mater. Chem.* **1998**, *8*, 1273.
(23) Hernandez, V. S.; Martinez, L. M. T.; Mather, G. C.; West, A. R. *J. Mater. Chem.* **1996**, *6*, 1533.
(24) Strobel, P.; Palos, A. I.; Anne, M.; Le-Cras, F. *J. Mater. Chem.* **2000**, *10*, 429.
(25) Hayashi, N.; Ikuta, H.; Wakihara, M. *J. Electrochem. Soc.* **1999**, *146*, 1351.
(26) Blasse, G. *J. Inorg. Nucl. Chem.* **1964**, *26*, 1473.
(27) Braithwaite, J. S.; Catlow, C. R. A.; Harding, J. H.; Gale, J. D. *Phys. Chem. Chem. Phys.* **2000**, *2*, 3841.
(28) Blasse, G. *J. Phys. Chem. Solids* **1966**, *27*, 383.
(29) Lee, Y. J.; Eng, C.; Grey, C. P. *J. Electrochem. Soc.* **2001**, *148*, A249.
(30) Joubert, J. C.; Durif, A. *C. R. Acad. Sci. Paris* **1964**, *258*, 4482.

magnetic field strengths to reduce the dipolar couplings between the electronic and nuclear magnetic moments.

Both $^6$Li and $^7$Li NMR have been employed to study various lithium manganates and lithium nickel cobaltates, before and after electrochemical cycling. Large hyperfine shifts are typically seen for the paramagnetic materials,[31−35] which provide information concerning the local environments (crystallographic and electronic) of the lithium ions. For example, we have previously identified the Li NMR signatures for different Li environments in many of these compounds.[31] Li cations in the octahedral site of the manganese-containing spinel structure give rise to a resonance at ∼2000 ppm for Mn(IV) compounds, while lithium in the tetrahedral sites of $Mn^{3+}$, $Mn^{3.5+}$, and $Mn^{4+}$ compounds results in shifts of 100−850 ppm, the size of the shift increasing as a function of the manganese oxidation state.[31]

In this work, we investigate the effect of the Zn substitution on the local lithium environments and the long-range structures of Zn-doped lithium manganese oxide spinels $LiZn_xMn_{2-x}O_4$. The cation distributions, the cation ordering at the $x = 0.5$ composition, and the limits of solid solution in the range $0 < x \leq 0.5$ are explored. The structure of $LiZn_{0.5}Mn_{1.5}O_4$ is determined by neutron powder diffraction (NPD) to confirm the ordering schemes proposed in the earlier XRD studies. The change in the local structure during charging (for $x = 0.1$) is examined to correlate the electrochemical properties (e.g., the potential profiles) with changes in local structure.

## Experimental Section

**Sample Preparation.** $LiZn_xMn_{2-x}O_4$ ($x = 0.1$, 0.2, 0.3, and 0.5) samples were synthesized in either air or an $O_2$ atmosphere by conventional solid-state reactions. Pelletized mixtures of $Li_2CO_3$, $MnCO_3$, and ZnO were heated at 700 °C for 48 h with intermittent grinding and were slowly cooled to room temperature at a controlled cooling rate of 1 °C min$^{-1}$. The $x = 0.5$ samples were also quenched from high temperature. These samples were calcined at 750 °C for approximately 24 h in air and then quickly cooled to room temperature by dropping the samples in water. $^6$Li-enriched samples were synthesized with $^6$Li-enriched $Li_2CO_3$ (Isotec; $^6$Li > 95%) for the variable temperature NMR and charging experiments.

**X-ray and Neutron Powder Diffraction.** All the samples were characterized with a Scintag powder X-ray diffractometer. X-ray powder diffraction data for $LiZn_{0.5}Mn_{1.5}O_4$ were collected at the National Synchrotron Light Source (NSLS) at Brookhaven National Laboratory. To index the unit cell and determine the space group symmetry, high-resolution synchrotron powder diffraction data were collected using a flat quartz sample holder at the X3B1 beam line ($\lambda = 1.15006$ Å; step size = 0.005° ($2\theta$); range of $5° < 2\theta < 55°$). NPD data were collected for the structure refinement of $LiZn_{0.5}Mn_{1.5}O_4$ with the 32 detector BT-1 neutron powder diffractometer at the National Institute of Standards and Technology (NIST) Center for Neutron Research, NBSR reactor. Measurements were performed at ambient conditions using a Cu(311) monochromator with $\lambda = 1.540(1)$ Å and step size = 0.05° ($2\theta$). The GSAS (General Structure Analysis System)[36] program suite was used for the Rietveld structure refinement.

**Solid-State NMR Spectroscopy.** $^6$Li MAS NMR spectra were acquired at 29.47 MHz on a CMX-200 spectrometer with a Chemagnetics probe equipped with a 4 mm (o.d.) rotor. Approximately, 150 mg of sample was loaded into the rotors, except for the experiments performed on the cycled samples where only approximately 20 mg was available. All spectra were obtained with an echo pulse sequence ($90° - \tau - 180° - \tau -$ acq.) at spinning speeds of 15−18 kHz. The pulse sequence was rotor-synchronized with a $\tau$ value being chosen as one rotor period (=1/spining speed). All spectra were referenced to a 1 M LiCl solution, at 0 ppm. A $\pi/2$ pulse length of 2.8 $\mu$s and a delay time of 0.2−0.5 s were used. Variable temperature NMR experiments were performed with the Chemagnetics variable temperature stack. Due to frictional heating at high spinning speeds, the actual temperature at the sample is higher than the temperature setting by 20−30 °C. Thus, temperature was calibrated with $Pb(NO_3)_2$ for the temperature range and the spinning speeds used in this study and the calibrated (actual) temperatures are given in the spectra and the text.

**Electrochemical Studies.** The cathodes were prepared by mixing $LiZn_xMn_{2-x}O_4$, graphite (TIMCAL America, SFG 15), acetylene black, and poly(vinylidene fluoride) (PVDF) binder in the weight ratio of 80:7.5:7.5:5. The mixture was slurried in 1-methyl-2-pyrrolidinone solvent and then doctor-bladed onto an aluminum foil. The solvent was evaporated at 60 °C for 1 h. A cathode disk was punched out from the coated Al foil and was weighed. The disks contained approximately 20 mg of active material. The cathode and lithium foil anodes were assembled in a swagelock-type cell with a Celgard separator and filter paper. A solution of $LiPF_6$ (1.0 M) in a mixture of ethylene carbonate (EC) and dimethyl carbonate (DMC) (1:1 v/v) was used as an electrolyte. The sample was cycled at a current rate of approximately C/7 between cutoff potentials of 3.3−4.5 V. After the cell was charged to a desired level, it was disassembled for the subsequent NMR experiments. The extracted cathodes were washed with alcohol and acetone to remove the electrolyte residue. The amount of lithium deintercalation was calculated from the total number of coulombs passed and the weight of the active materials.

## Results

**X-ray Powder Diffraction.** The presence of a cubic spinel phase was confirmed for all the samples by comparing the diffraction patterns obtained on the laboratory X-ray diffractometer with those in the Joint Committee on Powder Diffraction Standards. $Li_2MnO_3$ was detected as an impurity phase in both the $x = 0.5$ samples but not in the other samples. Additional diffraction lines, which could be indexed to the space group $P2_13$ (see below), were observed for the $x = 0.5$ material slowly cooled from 700 °C to room temperature. This superstructure is ascribed to a 1:3 ordering of Li and Mn over the octahedral sites and a 1:1 ordering of Li and Zn over the tetrahedral sites, consistent with the previous study.[26] The XRD pattern of the $x = 0.5$ sample quenched from 750 °C was indexed to a cubic spinel phase with a space group $Fd\bar{3}m$, indicating the absence of long-range cation ordering in either the tetrahedral site or octahedral site of the spinel structure. However, the (220) Bragg reflection increased in intensity, with increasing $x$, confirming the occupancy of Zn in the tetrahedral sites.[37,38] For the $x = 0.3$ sample, some peak

(31) Lee, Y. J.; Wang, F.; Grey, C. P. *J. Am. Chem. Soc.* **1998**, *120*, 12601.
(32) Morgan, K. R.; Collier, S.; Burns, G.; Ooi, K. *J. Chem. Soc., Chem. Commun.* **1994**, 1719.
(33) Mustarelli, P.; Massarotti, V.; Bini, M.; Capsoni, D. *Phys. Rev. B* **1997**, *55*, 12018.
(34) Marichal, C.; Hirschinger, J.; Granger, P.; Ménétrier, M.; Rougier, A.; Delmas, C. *Inorg. Chem.* **1995**, *34*, 1773.
(35) Gee, B.; Horne, C. R.; Cairns, E. J.; Reimer, J. A. *J. Phys. Chem. B* **1998**, *102*, 10142.
(36) Larson, A. C.; Von-Dreele, R. B. *GSAS General Structure Analysis System*; Los Alamos National Laboratory: Los Alamos, NM, 1995.
(37) Wolska, E.; Stempin, K.; Krasnowska-Hobbs, O. *Solid State Ionics* **1997**, *101−103*, 527.

**Table 1. Final Atomic Parameters[a] of Ordered $LiZn_{0.5}Mn_{1.5}O_4$ from Rietveld Refinement[b] Analysis Using Neutron and Synchrotron X-ray Powder Diffraction Data**

| atom | Wyckoff site | *x* | *y* | *z* | $U_{iso}$ | occupancy neutron; [X-ray] |
|---|---|---|---|---|---|---|
| Mn(1) | 12b | 0.1185(9) | 0.1167(7) | −0.368(1) | 0.009(1) | 1.0(1); [0.996(7)] |
| Zn(1) | 4a | 0.2464(8) | 0.2464(8) | 0.2464(8) | 0.013(1) | 0.95(1); [0.948(5)] |
| Li(1) | 4a | −0.0010(9) | −0.0010(9) | −0.0010(9) | 0.008(3) | 0.79(4) |
| Li(2) | 4a | 0.373(3) | 0.127(2) | −0.127(2) | 0.020(5) | 1.0(1) |
| O(1) | 12b | 0.0981(5) | 0.1318(4) | 0.3936(5) | 0.002(1) | 1; [0.95(1)] |
| O(2) | 12b | 0.3768(7) | 0.8513(6) | 0.3624(6) | 0.024(1) | 1; [1.01(1)] |
| O(3) | 4a | 0.3825(4) | 0.3825(4) | 0.3825(4) | 0.010(9) | 1; [1.08(3)] |
| O(4) | 4a | −0.1392(6) | −0.1392(6) | −0.1392(6) | 0.015(2) | 1; [0.96(3)] |

[a] Space group $P2_13$ and $a = 8.1823(1)$ Å obtained from analysis of the synchrotron X-ray powder diffraction data. [b] Discrepancy indices: $wR_p = 0.041$, $R_p = 0.033$, $R(F^2) = 0.049$, and $\chi^2 = 2.0$.

broadening was observed, reflecting a distribution in Zn concentrations. Additional weak diffraction lines, which could again be indexed with the space group of $P2_13$, were observed, but the intensity of these reflections was weaker than those observed for the $x = 0.5$ sample.

**Structure Refinement of $LiZn_{0.5}Mn_{1.5}O_4$.** Neutron diffraction and X-ray synchrotron data were collected for the structural refinement of ordered $LiZn_{0.5}Mn_{1.5}O_4$. The majority of peaks in the synchrotron X-ray and neutron diffraction patterns were indexed on the basis of a cubic unit cell with space group symmetry of $P2_13$, a subgroup of the disordered form of $LiZn_{0.5}Mn_{1.5}O_4$ ($Fd\bar{3}m$).[26,30] Subgroups $F4_132$, $P4_132$, and $F23$ were excluded on the basis of the presence of reflections (002), (006), (011), (012), (112), and (013). No discernible peak splittings or differences in the widths of the ($h$00) and ($hhh$) reflections at comparable values of $2\theta$ were observed, and hence there is no evidence for a further lowering of the symmetry from cubic to tetragonal. The model with ordering of the Li and Zn cations in the tetrahedral sites and of the Li and Mn cations in the octahedral sites served as a starting model for the Rietveld analysis with the neutron diffraction data. Initially, Li cations were presumed to occupy both the tetrahedral and octahedral positions (the Wyckoff site positions 4a in Table 1), and Mn was presumed to occupy only the octahedral positions 12b. The profile parameters (zero point, lattice parameters, peak widths, and peak forms) were optimized by using a Le Bail refinement.[39] These parameters were then fixed during the initial refinements of the structure model and released in the final stages. The refined $Li_2MnO_3$/$LiZn_{0.5}Mn_{1.5}O_4$ ratio of 1:7 (by formula unit) was determined from the scale factors.

Following refinement of the positional parameters for oxygen and zinc, a Fourier-difference synthesis revealed positions for the octahedrally coordinated Mn1 and tetrahedrally coordinated Li1 sites (Table 1) as regions of negative density. Subsequent refinements and Fourier calculations revealed the position of the second octahedrally coordinated site designated as Li2 in Table 1. Unconstrained refinement of the site population parameters for the Mn1, Zn1, Li1, and Li2 sites, assuming that they are occupied exclusively by Zn, Mn, and Li and that the oxygen sites are fully occupied, are summarized in Table 1 and Figure 1. The local environments of the tetrahedral and octahedral Li1 and Li2 sites are shown in Figure 2.

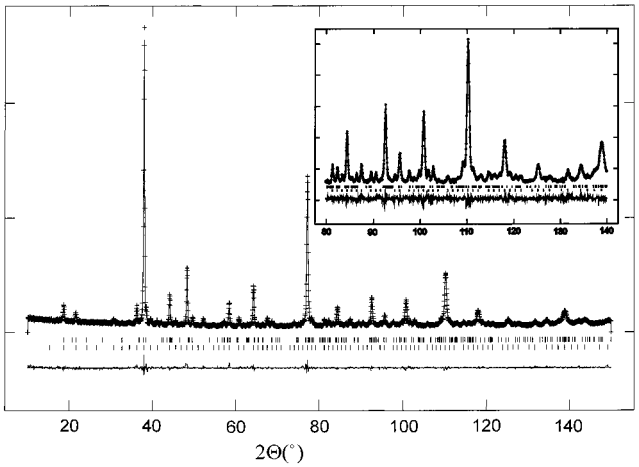


**Figure 1.** Computed (line) and observed (crosses) neutron powder diffraction patterns for ordered $LiZn_{0.5}Mn_{1.5}O_4$ and the crystallographic model (Table 1). The lower and upper sets of short vertical lines indicate reflections for $LiZn_{0.5}Mn_{1.5}O_4$ and the $Li_2MnO_3$ impurity, respectively. The lower curve shows the difference between the observed and calculated data plotted on the same scale.

The octahedrally coordinated sites Mn1 and Li2 are fully occupied, while the tetrahedrally coordinated sites Li1 and Zn1 have occupancies of 95 and 80%, respectively. Note that this may indicate some disorder between the Li and Zn sites, since Li and Zn have scattering factors of opposite sign. For example, it is difficult to differentiate between occupancies of 0.05 Zn and 0.95 Li on the Li1 site vs 0.8 Li, with both these occupancies resulting in similar scattering.

The synchrotron data provided an opportunity to test the uniqueness of the occupancies obtained by neutron diffraction, as the scattering contrast between Mn, Li, and Zn is different for X-rays and neutrons. Refinements of the occupancies of the sites populated by Mn and Zn by using the synchrotron XRD and NPD data are in good agreement (Table 1). The oxygen occupancies were then refined, while the rest of the other atomic parameters were fixed to the values obtained from the neutron data analysis. Note, however, that the neutron refinement was performed on a different sample than the sample used for the XRD, due to the need to synthesize additional material for the neutron experiment; thus, some caution must be exercised in analyzing the oxygen occupancies in particular. What is clear, however, is that there is a low level of residual disorder in this material.

**$^6$Li MAS NMR of $LiZn_xMn_{2-x}O_4$ ($x = 0.1-0.5$).** The $^6$Li MAS NMR spectra of $LiZn_xMn_{2-x}O_4$ ($x = 0.1$, 0.2, 0.3, 0.5), prepared by the slow cooling from 700 °C, are shown in Figure 3. All the spectra contain resonances,

(38) Woodley, S. M.; Catlow, C. R. A.; Piszora, P.; Stempin, K.; Wolska, E. *J. Solid State Chem.* **2000**, *153*, 310.
(39) Lebail, A.; Duroy, H.; Fourquet, J. L. *Mater. Res. Bull.* **1988**, *23*, 447.

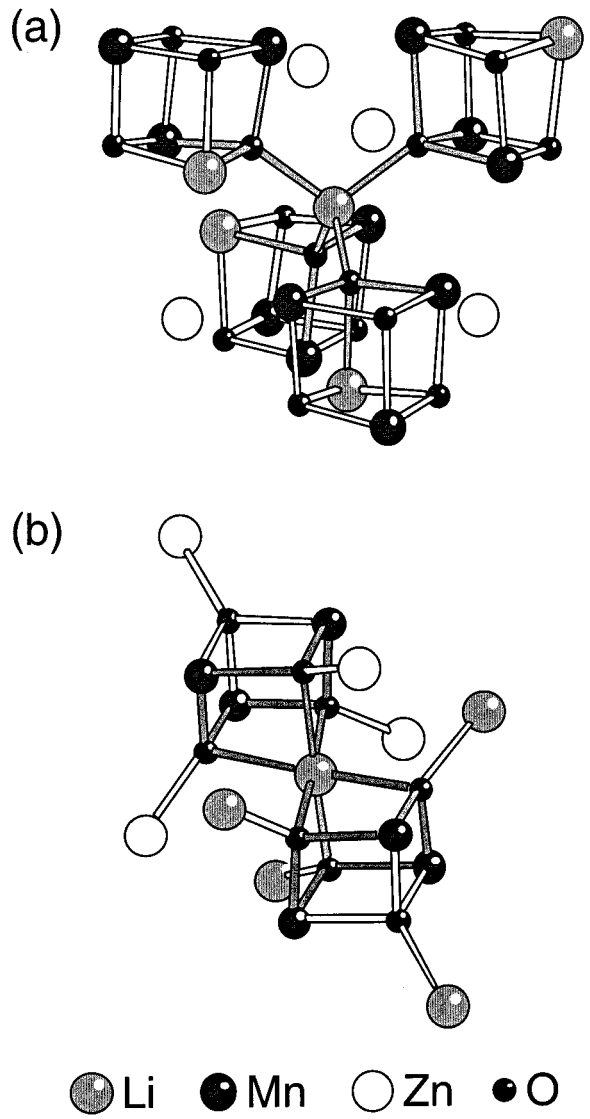


**Figure 2.** Local coordination environment of lithium in (a) the tetrahedral site Li1 and (b) the octahedral site Li2 in the ordered structure of $LiZn_{0.5}Mn_{1.5}O_4$. The Li−O−Mn/Li bonds involving the central lithium atom are shaded.

with large associated spinning sidebands, that are shifted by 500−2300 ppm from the typical chemical-shift position of diamagnetic solids (at close to 0 ppm), due to the hyperfine interaction. For the samples with Zn-doping levels of $x = 0.1$ and 0.2, at least four resonances are observed at 502, 573, 649, and 718 ppm and 482, 547, 630, and 704 ppm with approximate intensity ratios, obtained by deconvolution of the spectra of 5:18:11:8 and 5:22:28:20, respectively. On the basis of earlier work, all these resonances are assigned to lithium in the tetrahedral site of the spinel structure.[29,31] A weaker resonance at approximately 2100 ppm is also observed, which is assigned to Li in the octahedral site, again based on our previous studies.[29,31] The spectrum of the $x = 0.3$ sample shows resonances in two distinct frequency ranges, one at around 2331 ppm due to octahedral Li cations and the other consisting of several overlapping resonances at 500−750 ppm. The latter group of resonances were deconvoluted yielding five separate peaks at 501, 571, 669, 690, and 748 ppm, with an intensity ratio of 3:11:23:16:16. Among these, the resonance at 690 ppm is considerably narrower. Two

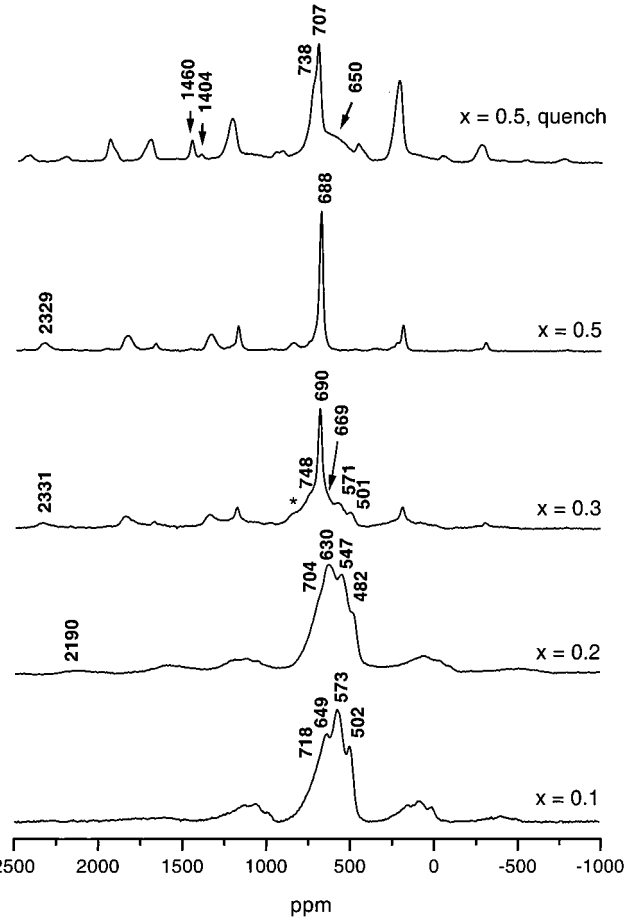


**Figure 3.** $^6$Li MAS NMR spectra of $LiZn_xMn_{2-x}O_4$ ($x = 0.1$, 0.2, 0.3, 0.5) synthesized in air. For $x = 0.5$, both the slowly cooled and quenched samples are shown. A spinning speed, $\nu_r$, of 17 kHz was used for the $x = 0.2$ sample, while ~15 kHz was used for the others. Isotropic resonances are marked on the spectra, and all other peaks are spinning sidebands; some of the spinning sidebands (one spectrum and in the subsequent figures) have been marked with "*"s, particularly when the hyperfine shifts of the sidebands fall in the typical range expected for the isotropic resonances.

major $^6$Li resonances at 688 and 2329 ppm are seen for the $x = 0.5$ compound, along with weaker resonances at 720 and 742 ppm. Again, the broad resonance at 2329 ppm has a wide, asymmetric spinning sideband manifold spanning approximately 130 kHz and is assigned to octahedral Li ions. The $^6$Li MAS NMR spectrum of $LiZn_{0.5}Mn_{1.5}O_4$ quenched from a calcination temperature of 750 °C is also shown in Figure 3. Additional resonances at 707, 1404, and 1460 ppm are now observed along with a very broad resonance centered at around 650 ppm.

**Variable Temperature $^6$Li MAS NMR.** NMR experiments were performed for $LiZn_xMn_{2-x}O_4$ ($x = 0.1$, 0.3, and 0.5) samples that were prepared by slow cooling from 700 °C in an $O_2$ atmosphere (Figures 4−6). These samples were prepared to explore the effect of the oxygen partial pressure on cation ordering and the limits of solid solution. However, at room temperature, no discernible differences were noted by NMR spectroscopy between these samples and those prepared in an air. For $LiZn_{0.1}Mn_{1.9}O_4$ (Figure 4) the four resonances assigned to Li in the tetrahedral sites shift to lower frequency and collapse, one by one, into a single resonance as the temperature increases. By 283 °C, a

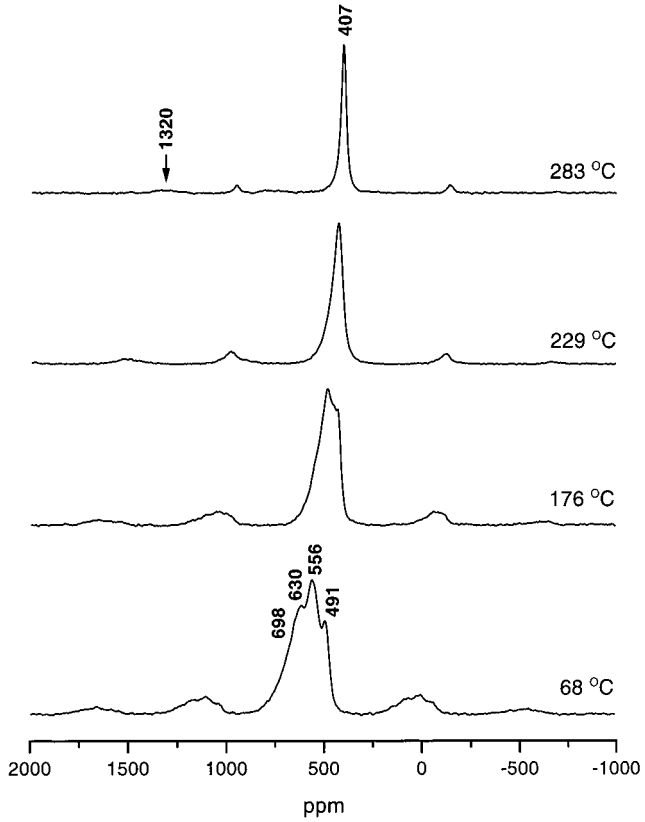


**Figure 4.** Variable temperature $^6$Li MAS NMR spectra for $LiZn_{0.1}Mn_{1.9}O_4$ synthesized under an oxygen atmosphere. The actual sample temperature, obtained from the temperature calibration, is marked on the spectra; $\nu_r = 16$ kHz.

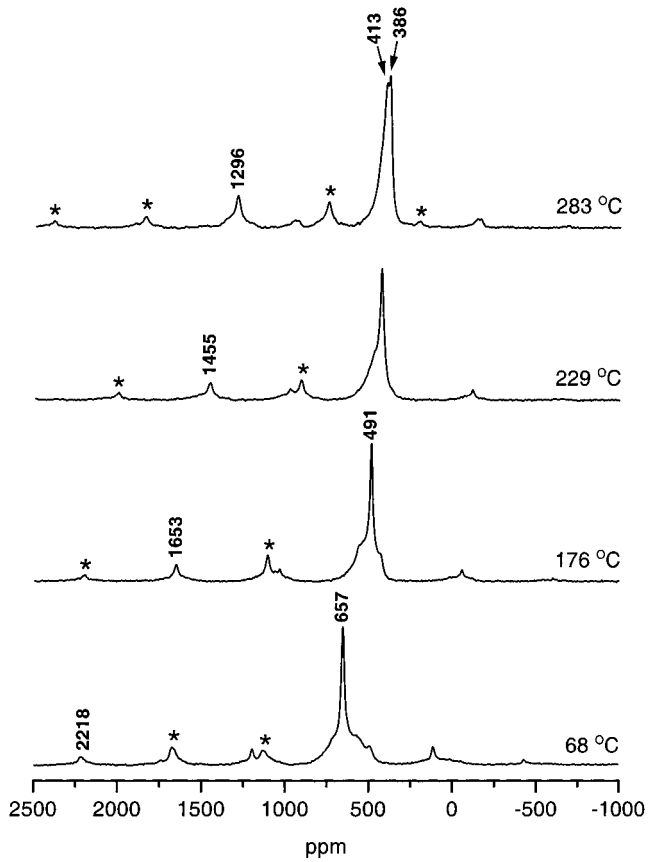


**Figure 5.** Variable temperature $^6$Li MAS NMR spectra of $LiZn_{0.3}Mn_{1.7}O_4$ synthesized under an oxygen atmosphere; $\nu_r = 16$ kHz.

single, narrow resonance at 407 ppm with a shoulder at high frequency remains and a resonance at 1320 ppm with a broad spinning sideband manifold, due to Li cations in the octahedral site, is clearly seen. The shift of the resonances to lower frequency with increasing temperature is consistent with a decrease in magnetic susceptibility. $LiZn_{0.3}Mn_{1.7}O_4$ shows a slightly different behavior (Figure 5). As the temperature increases, a shift to lower frequency, accompanied by coalescence, is still observed. However, the coalescence is no longer complete even at the highest temperature studied, and at 283 °C, two resonances at 386 and 413 ppm can still be clearly resolved. The $^6$Li NMR resonances of $LiZn_{0.5}Mn_{1.5}O_4$ also shift to lower frequency with increasing temperature (Figure 6), but the weaker, high-frequency peaks do not collapse into the resonance due to the tetrahedral lithium ions at high temperatures. For both the $x = 0.3$ and 0.5 samples, the resonance due to Li in the octahedral site shifts to lower frequency as the temperature increases, and the width of its spinning sideband manifolds decreases. However, resonances assigned to Li in the octahedral and tetrahedral sites do not coalesce, even at 283 °C. All the resonances shift to higher frequency and broaden below room temperature.

**$^6$Li NMR Spectra following Charging.** The potential profile of the $LiZn_{0.1}Mn_{1.9}O_4$ cathode during the first charging and discharging cycle is shown in Figure 7. In contrast to the $LiMn_2O_4$ spinel, a two-step potential profile is no longer seen. An initial charge capacity of 84 mAh $g^{-1}$ in the ~4.18 V region and a discharge capacity of 75 mAh $g^{-1}$ are obtained. Although this initial capacity is low, improved capacity retention over that of our samples of stoichiometric $LiMn_2O_4$ is seen after 20 cycles, of 83 and 78 mA h $g^{-1}$ for charging and discharging, respectively. For $LiZn_{0.5}Mn_{1.5}O_4$, no capacity was obtained in the 4−5 V region. Instead, only electrolyte decomposition was observed at ~5 V.

Figure 8 shows $^6$Li MAS NMR spectra of the $LiZn_{0.1}Mn_{1.9}O_4$ cathode charged to different extents. As charging proceeds, the intensity of the $^6$Li signal decreases, due to the removal of lithium from the compound. When charged to 14%, no fine structure remains, leaving a resonance at 581 ppm. As the extent of charging increases further, the resonance gradually shifts to higher frequency and broadens, consistent with an increase in average Mn oxidation state. A new resonance starts to appear at 822 ppm when the charging level reaches 70%. When the charging level is close to 100%, of which corresponds to a final stoichiometry $Li_{0.46}Zn_{0.1}Mn_{1.9}O_4$, the original resonance, now shifted to 643 ppm, and the new resonance at 822 ppm are observed. The resonance due to octahedral Li is seen throughout the whole charging range, shifting slightly from approximately 2100 to 2200 ppm on charging.

## Discussion

**The Disordered Phases: $LiZn_xMn_{2-x}O_4$ ($x = 0.1$, 0.2).** At least three additional resonances (at 550−700 ppm), due to tetrahedral Li, are observed for $LiZn_xMn_{2-x}O_4$ for $x = 0.1$ and 0.2 in addition to the resonance at ~500 ppm, from the normal spinel environment.[31] The intensities of these additional resonances progres-

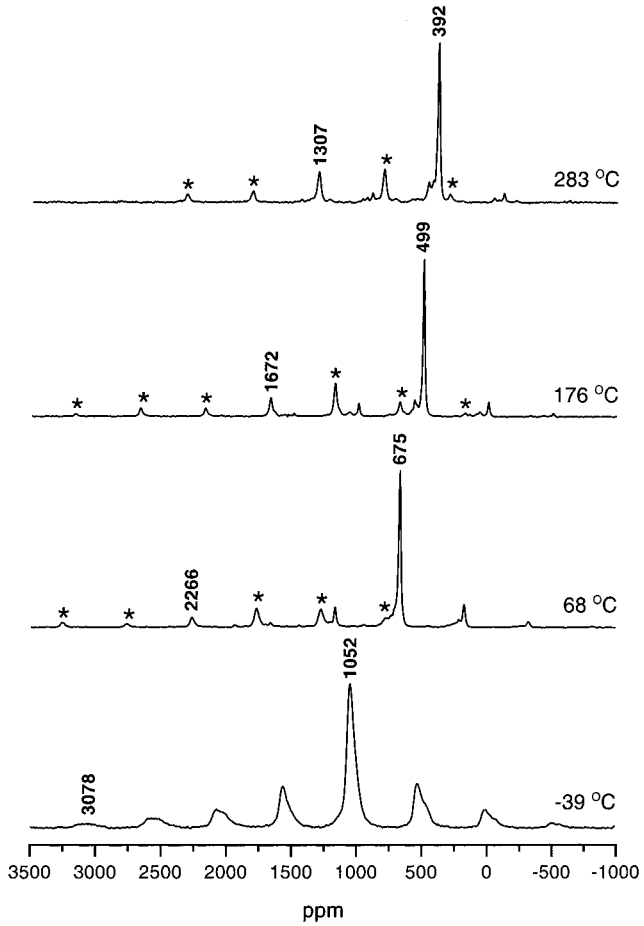


**Figure 6.** Variable temperature $^6$Li MAS NMR spectra of $LiZn_{0.5}Mn_{1.5}O_4$ synthesized under an oxygen atmosphere; $\nu_r$ = 15 kHz.

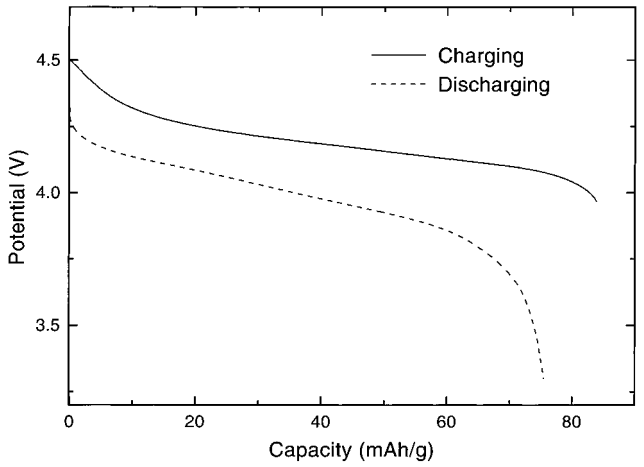


**Figure 7.** Potential profile of the $LiZn_{0.1}Mn_{1.9}O_4$ cathode obtained during the first charging and discharging.

sively increase and the center of mass shifts to higher frequency, with increased Zn-doping level. Previous NMR studies have shown that the predominant mechanism responsible for the large Li NMR shifts in lithium manganese oxides is the Fermi-contact (or hyperfine) interaction[31,33,35,40]

$$H_c = I_z A_s \langle S_z \rangle \quad (1)$$

where $A_s$ is the hyperfine coupling constant and $\langle S_z \rangle$ is the thermally averaged value of the electronic spin.

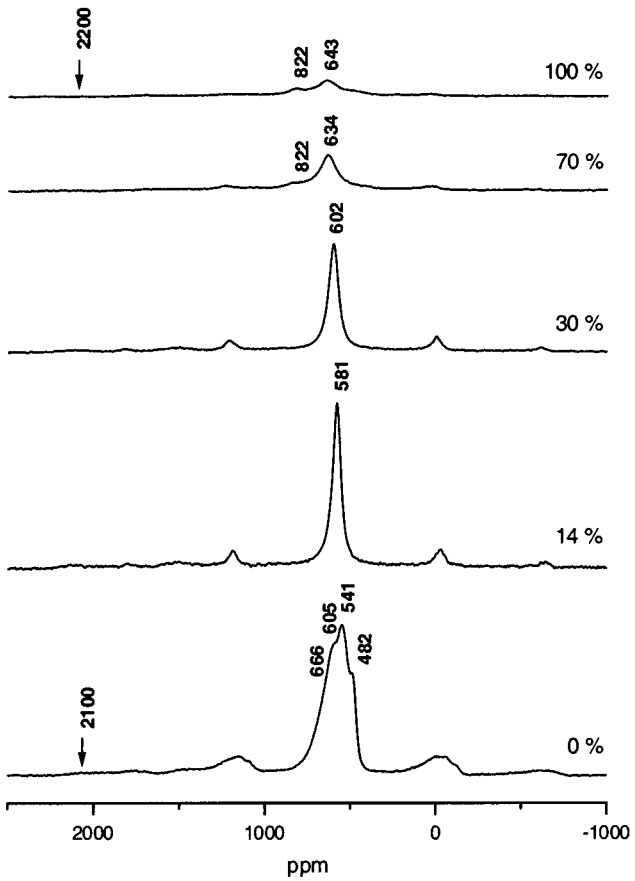


**Figure 8.** $^6$Li MAS NMR spectra of $LiZn_{0.1}Mn_{1.9}O_4$ during the first charge. The isotropic resonance and the extent of charging are marked on the spectra. The spectra are plotted in an absolute intensity scale, taking into account the mass of the active material and the number of acquisitions; $\nu_r$ = 18 kHz.

$\langle S_z \rangle$ is directly proportional to the magnetic susceptibility. Li NMR hyperfine shifts are sensitive to the oxidation state of nearby manganese *and* the local structure, a shift to higher frequency being observed as the manganese oxidation state increases.[31,41] Thus, the shift to higher frequency, with increasing Zn concentration, is consistent with an increase in manganese oxidation state.

The discrete resonances seen on Zn doping, which are separated by ~70 ppm, are assigned to Li ions in different local environments, due to different numbers of $Mn^{3+}$, $Mn^{4+}$, and $Zn^{2+}$ ions in their local coordination spheres. The simplest explanation for these additional resonances is that they arise from the presence of substituted cations (in this case, $Zn^{2+}$) in the local coordination sphere of Li. However, the substitution of a manganese cation, with an average oxidation state of $Mn^{3.5+}$, by $Zn^{2+}$ is very unlikely to cause a *larger* Fermi-contact shift, since $Zn^{2+}$ ($d^{10}$) is diamagnetic. We have observed a similar series of $^6$Li NMR resonances on substituting $Ni^{2+}$ into $LiMn_2O_4$ spinels, with both similar separations between resonances and similar intensities.[29] Additional resonances (albeit with slightly different frequency separations and intensities) were seen in the spectra of lithium-excess spinel materials

(40) McConnell, H. M.; Robertson, R. E. *J. Chem. Phys.* **1958**, *29*, 1361.
(41) Lee, Y. J.; Grey, C. P. *Chem. Mater.* **2000**, *12*, 3871.

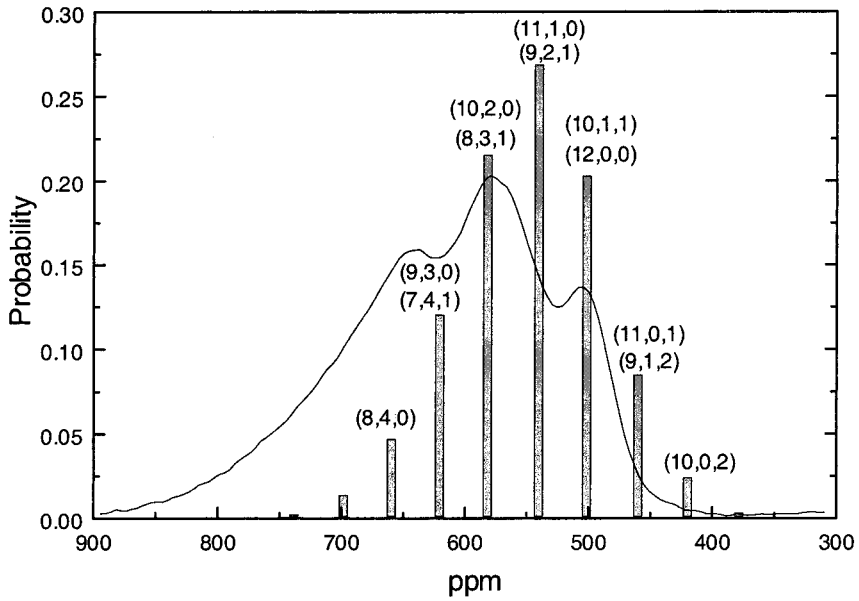


**Figure 9.** Histogram of the approximate Li NMR frequencies and intensities for $LiZn_{0.1}Mn_{1.9}O_4$ estimated from the random distribution model. The different local coordination environments that give rise to the various frequencies are labeled on the corresponding resonances (as no. of $Mn^{3.5+}$, $Mn^{4+}$, and $Li^+$ ions). The NMR spectrum of $LiZn_{0.1}Mn_{1.9}O_4$ is also shown for comparison.

(e.g., $Li_{1.05}Mn_{1.95}O_4$) and samples synthesized at low temperatures ($Li_{1-\delta}Mn_{2-2\delta}O_4$).[31] The similarity in the spectra, irrespective of the type of defect or dopant (particularly for $Ni^{2+}$ and $Zn^{2+}$), suggests that it is the presence of manganese cations with an average oxidation state of greater than $Mn^{3.5+}$ in the Li local coordination sphere that is responsible for these new peaks. The introduction of each $Zn^{2+}$ results in the oxidation of three manganese ions with an average oxidation state of $Mn^{3.5+}$ to $Mn^{4+}$. The electron holes introduced by this $Zn^{2+}$ substitution do not appear to be delocalized throughout the lattice but are rather localized on individual manganese ions, at least at room temperature. Thus, the resonance at ~500 ppm is assigned to Li ions in the tetrahedral site surrounded by 12 $Mn^{3.5+}$ ions in their first cation coordination sphere. The additional resonances are then assigned to Li with increasing numbers of $Mn^{4+}$ in their nearest coordination sphere. (See Figure 2 for the local arrangement of octahedrally coordinated cations around a central tetrahedral site.)

The probability of each tetrahedral local environment in $LiZn_{0.1}Mn_{1.9}O_4$ can be readily calculated by assuming a random substitution of $Li^+$, $Mn^{4+}$, and $Mn^{3.5+}$ ions on the octahedral sites. On the basis of our earlier work, the size and the direction of Li NMR shift can be estimated by considering the types of orbital overlap and the number of manganese ions in the first and second cation coordination sphere when there are no strong magnetic interactions between electronic spins; the lithium cations in the spinel structure are coordinated to nearby manganese ions via intervening oxygen atoms with Li−O−Mn bond angles of approximately 122°. Each Li−O−Mn interaction has been shown to give rise to an additive shift of 60−81 ppm in lithium manganese(IV) spinels and 42 ppm for $Mn^{3.5+}$ spinels.[31] To simulate the spectrum predicted for a random distribution of $Mn^{4+}$ ions, a shift of 81 ppm, corresponding to the value for each Li−O−Mn 122° bond in $Li_4Mn_5O_{12}$, was used. The intensities and estimated shifts are shown in Figure 9 and are quite different from those in the observed spectrum, particularly in the high-frequency region; better fits to the spectrum are not obtained with this random distribution model if different values for the Li−O−$Mn^{4+}$ shifts are used. This suggests that the electron holes produced on $Zn^{2+}$ doping are not randomly distributed in the lattice but must be clustered, presumably in the nearest cation coordination sphere of the $Zn^{2+}$ or $Li^+$ cations, due to electrostatic considerations. Local environments $Li(OLi)(OMn^{3.5+})_{11}$ and $Li(OLi)_2(OMn^{3.5+})_{10}$, which are predicted to give rise to resonances at lower frequency than those of the main spinel resonance (at approximately 500 ppm), do not appear to be present. One possible explanation for this is that the local tetrahedral environments such as $M(OLi)_x(OMn^{3.5+})_{12-x}$, M = $Li^+$ or $Zn^{2+}$, which are associated with an overall negative charge when compared to the average tetrahedral local environment of the bulk, tend to be favored by the doubly charged $Zn^{2+}$ cation and not $Li^+$, again in order to achieve optimal local charge balance. This implies that lithium will preferentially substitute in tetrahedral local environments such as $Li(OMn^{4+})_2(OMn^{3.5+})_{10}$, resulting in greater intensity to higher frequency of the normal spinel site than predicted by the random model and as observed experimentally (Figure 9). Furthermore, we have postulated that lithium substitution into the octahedral site of the spinel structure is always accompanied by oxidation of *nearby* $Mn^{3.5+}$ ions to $Mn^{4+}$; thus, arrangements such as $Li(OLi)(OMn^{3.5+})_{11}$ will always be disfavored. A number of factors appear to be responsible for the observed distributions of cations, but three points are very clear: (1) the $Li^+$ and $Zn^{2+}$ are not arranged randomly in the lattice, (2) the electron holes are at least partially localized, and (3) $Li^+$ prefers local environments near $Mn^{4+}$ (i.e., the electron holes are located preferentially near $Li^+$).

As the amount of Zn doping increases, the intensity of the resonance due to the lithium in the octahedral site increases due to the gradual substitution of Li into the octahedral sites, leading to the cation distribution $(Li_{1-x}Zn_x)_{Td}[Mn_{2-x}Li_x]_{Oh}O_4$. This is consistent with the

preference of Zn for tetrahedral coordination. As seen more clearly in the spectra of the $x = 0.3$ and 0.5 compounds, a large anisotropic interaction, caused by the dipolar coupling between electronic and nuclear spins, results in very wide spinning sideband manifolds. Since the dipolar coupling between two spins is inversely proportional to the cube of the distance between the spins, much larger sidebands are expected for lithium in the octahedral sites than in the tetrahedral sites (see Figure 3), consistent with experimental observations. As a result of the large dipolar coupling, the intensity of the isotropic resonance is severely attenuated. However, the dipolar coupling decreases at elevated temperatures due to the reduced time-averaged magnetic moments of the spins (i.e., the atomic susceptibility), and consequently the intensity of the isotropic peak grows, relative to the intensity contained in the spinning sidebands. Hence, the 16d Li resonance is more readily detected in the NMR spectra acquired at higher temperatures.

A question still remains: why does the Li in the octahedral site in a compound with an average manganese oxidation state of less than +4 still give rise to a resonance at ~2000 ppm? This in part must be due to the fact that there is no direct or two-bond overlap interaction between the $e_g$ orbital of Mn and the s orbital of Li, when mediated by an oxygen 2p orbital through a 90° interaction. Thus, the Li in the octahedral site is not affected, to a first approximation, by the electrons in the $e_g$ orbitals of Mn. A second possibility is that all or many of the manganese ions surrounding the Li cations in the octahedral site are oxidized to $Mn^{4+}$, consistent with our view of localized electron holes near the substituted $Li^+$ ions.

**$LiZn_{0.3}Mn_{1.7}O_4$.** One sharp and four broad resonances are observed for the $x = 0.3$ sample. The sharp resonance is identical to that seen in the Li NMR spectrum of the $x = 0.5$ ordered sample, while the broad resonances are similar to those of the $x = 0.2$ compound. The variable temperature NMR experiments are consistent with two coexisting phases. Thus, it is concluded that $LiZn_xMn_{2-x}O_4$ with $x = 0.3$ is a mixture of $LiZn_{0.2}Mn_{1.8}O_4$ and $LiZn_{0.5}Mn_{1.5}O_4$ phases instead of a single-phase solid solution. This phase segregation was not readily discernible by XRD, due to similarity of the unit cell parameters of the two phases. However, peak broadening and some weak additional reflections due to partial cation ordering were detected, consistent with a mixture of two phases. Taking into account the lithium distribution in both tetrahedral and octahedral sites, the Li NMR intensity ratio of the $x = 0.5$ and 0.2 components is 1:2, which is consistent with the expected value based on the sample stoichiometry. The existence of a miscibility gap between the $x \cong 0.2$ and 0.5 components is presumably driven by the favorable Madelung energy that can be achieved by cation ordering[42] vs the favorable entropy terms gained by disorder. The increase in Madelung energy due to cation ordering will be the largest for the $x = 0.5$ phase, leading to a region of phase instability for samples synthesized under the conditions used in this study.

(42) Greenwood, N. N. *Ionic crystals, lattice defects and nonstoichiometry*; Butterworth: London, 1968.

**$LiZn_{0.5}Mn_{1.5}O_4$: Ordered vs Disordered Phases.** The cation ordering in $LiZn_{0.5}Mn_{1.5}O_4$ is sensitive to the synthesis condition, consistent with earlier work.[26,30] In the ordered structure ($P2_13$ space group) shown in Figure 2, each lithium ion in the tetrahedral site is coordinated to nine Mn and three Li cations through intervening oxygen with a bond angle close to 120.4°. Each lithium ion in the octahedral site is coordinated to six manganese ions via 12 Li−O−Mn linkages, with a 92.7° bond angle. Since the 121° and the 90° Li−O−Mn bond angles have been shown to contribute shifts of 60−80 and 150−170 ppm, respectively,[31] shifts of ≈630 and ≈2000 ppm are predicted for lithium in the tetrahedral and octahedral sites, respectively, for the ordered $Li_{0.5}Zn_{0.5}[Mn_{1.5}Li_{0.5}]O_4$, in good agreement with the experimentally observed shifts (688 and 2329 ppm).

Additional weak resonances at approximately 700−740 ppm are observed for the ordered samples synthesized in both air and oxygen. Unlike those in the $x = 0.1$ and 0.2 samples, the additional resonances seen in the $x = 0.5$ sample do not collapse into the resonance assigned to the Li in the tetrahedral sites, at high temperatures. This suggests that these resonances cannot be assigned to a small degree of disorder in the ordered $Li_{0.5}Zn_{0.5}[Mn_{1.5}Li_{0.5}]O_4$ phase. The additional resonances are assigned to $Li_2MnO_3$ (see below), consistent with the NPD refinement, which reveals that this sample contains approximately 14% $Li_2MnO_3$ as an impurity.

The sharp and broader resonances at 500−800 ppm in the $^6$Li NMR spectrum of the quenched sample appear to arise from very different sites. The intensities of the spinning sidebands of the sharper resonances are much larger than those typically observed for lithium in the tetrahedral site of the spinel. These resonances are, therefore, assigned to lithium in the octahedral sites between the transition-metal layers of $Li_2MnO_3$, consistent with the XRD results for this sample, where $Li_2MnO_3$ was identified as an impurity. Two earlier Li NMR studies of $Li_2MnO_3$ reported three resonances at 905, 922, and 1817 ppm and 850, 875, and 1770 ppm, which were assigned to Li in the 4h, 2c, and 2b sites, respectively.[32,33] However, our $^6$Li NMR spectrum of $Li_2MnO_3$, prepared to confirm the assignment by a conventional solid-state reaction, contains three resonances at 741, 774, and 1492 ppm. One explanation for the large differences in hyperfine shifts between our current studies and the earlier reports may arise from the extreme sensitivity of these shifts to temperature. Due to the fast MAS used in our studies, our "room temperature" measurements typically correspond to approximately 68 °C. Thus, assuming a Curie law dependence of the shift, a hyperfine shift of approximately 1740 ppm is predicted for the higher frequency resonance at 20 °C. A second explanation for the differences between our results and previous studies may arise from the partial disorder that is sometimes observed in this material.[43,44] However, in our spectra, we do not observe the series of peaks (or broadening) of a pure phase of $Li_2MnO_3$ that might be expected in a disordered material, suggesting

(43) Strobel, P.; Lambert-Andron, B. *J. Solid State Chem.* **1988**, *75*, 90.

(44) Riou, A.; Lecerf, A.; Gerault, Y.; Cudennec, Y. *Mater. Res. Bull.* **1992**, *27*, 269.

that, at least locally, our materials are ordered. A random distribution of cations in the tetrahedral and octahedral sites is present in the quenched sample, and thus a large variety of local environments are predicted, giving rise to a broadening of the resonance (at approximately 650 ppm) from the tetrahedral lithium sites.

On the basis of both the NMR and NPD results, it appears that single-phase $LiZn_{0.5}Mn_{1.5}O_4$ is difficult to obtain by solid-state reaction at high temperature. The disproportionation reaction into a defect spinel and $Li_2MnO_3$ is often observed at high temperature, especially with the Li-excess composition.[25,45,46] Hence, both the defect-spinel phase and $Li_2MnO_3$ are likely to be formed for the metal-doped spinels following the reaction

$$LiZn_{0.5}Mn_{1.5}O_4 \rightarrow Li_{1-2\delta}Zn_{0.5}Mn_{1.5-\delta}O_{4-3\delta} + \delta Li_2MnO_3 \quad (2)$$

For example, for $\delta = 0.1$, the composition of the defect-containing spinel phase can be rewritten as $Li_{0.86}Zn_{0.54}Mn_{1.51}O_4$, presuming no or few oxygen vacancies. Furthermore, based on the complete occupancy of the octahedral sites, as observed by neutron diffraction, we can distribute the cations among the octahedral and tetrahedral sites yielding $(Zn_{0.54}Li_{0.37})_{tet}(Li_{0.49}Mn_{1.51})_{oct}O_4$. This provides an explanation for the apparent low occupancy of lithium on the tetrahedral site, as observed by diffraction, even for the ordered material. The apparent Zn deficiency (as observed by diffraction) is likely to result from partial disorder of Zn over the two tetrahedral sites.

**Variable Temperature NMR Experiments.** The coalescences of the resonances due to the tetrahedral lithium ions, at high temperature, can be explained by lithium cation motion and/or delocalization of electrons. Similar behavior was observed previously in $LiMn_2O_4$, prepared at low temperature, and Ni-doped spinels.[29,31] Lithium manganese oxides are hopping semiconductors, where the conduction is mediated by electron hopping between the $e_g$ orbitals of the neighboring manganese ions.[47,48] In the materials containing defects (i.e., cation vacancies and dopant metals), however, the $e_g$ orbitals in manganese cations near a defect are perturbed and raised by an amount $\Delta E$ ($> kT$), so that these orbitals are not involved in the electron hopping at room temperature. Thus, the fine structure of Li NMR results from the localization of electron holes and consequent oxidation of manganese ions. At high temperature, the thermal energy of electrons may be sufficient (i.e., $\Delta E$ approaches $kT$), so that the $e_g$ orbitals near the defect are gradually populated resulting in the coalescence of the resonances. We suggested that lithium-ion motion may also partially contribute to the coalescence phenomena in the Ni-doped materials, at high temperatures.[29] Similar behavior is expected for the Zn-doped spinels since they contain similar defects and the variable temperature behavior is very similar (Figures 4 and 5). Thus, the coalescence of the resonances in this system is also ascribed to a combination of lithium-ion motion and a gradual delocalization of the electron holes, as the temperature increases. Lithium-ion motion is certainly required to explain the lack of a series of different resonances resulting from environments containing different numbers of (octahedral) lithium cations in the local coordination sphere.

The magnetic susceptibility of these types of materials can be described empirically by the Curie−Weiss (CW) Law, $\chi = C/(T - \theta)$, where $C$ is the Curie constant and $\theta$ is the Weiss constant. The sign and the size of the Weiss constant are a measure of the nature and the magnitude of the correlations between electrons. $LiMn_2O_4$ is an antiferromagnet below 40 K, with a very large Weiss constant of between −337 and −260 K.[49,50] $LiZn_{0.5}Mn_{1.5}O_4$ shows CW-like behavior for the temperature range studied (up to ∼900 K) and ferromagnetic order below 22 K with a Weiss constant of +35 K.[28] For $Li_4Mn_5O_{12}$, ferromagnetic ordering was observed below 83 K,[49] while the delithiated spinel, $\lambda$-$MnO_2$, orders antiferromagnetically at 30−32 K.[51] In the compounds containing only $Mn^{4+}$ paramagnetic ions, the 90° Mn−O−Mn ferromagnetic interaction competes with antiferromagnetic Mn−Mn interaction across the common edge of the octahedra. When the lattice constant is not small enough for significant Mn−Mn overlap to take place, the ferromagnetic interaction, which involves Mn $t_{2g}$ and Mn $e_g$ orbitals, dominates. This is the case for $Li_4Mn_5O_{12}$ and $LiZn_{0.5}Mn_{1.5}O_4$. For $\lambda$-$MnO_2$, the $Mn^{4+}$−$Mn^{4+}$ antiferromagnetic interaction increases in relative importance, due to the small lattice parameter ($a = 8.04$ Å in comparison to 8.14 Å for $Li_4Mn_5O_{12}$).

The total observed Li NMR shift is a sum of the hyperfine shift (the temperature-dependent term), the diamagnetic shift, the Knight shift, and the (temperature-independent) van Vleck shift.[52] In these semiconductors, the diamagnetic shift, measured against the LiCl standard, is relatively small (a few ppm) and the Knight shift, caused by conduction electrons is negligible. Assuming that the other terms are small, the hyperfine shift in eq 1 can be written in terms of the temperature

$$1/\delta = C'(T - \theta) \quad (3)$$

where $C'$ is a constant, which is inversely proportional to the hyperfine coupling. The inverse of the shift of the center of mass of the Li resonance vs temperature has been plotted in Figure 10 for $LiZn_xMn_{2-x}O_4$, with $x = 0.1$, 0.3, and 0.5. Since the sample with $x = 0.3$ stoichiometry contains two phases, the Li NMR shift has been analyzed separately for the $x = 0.2$ and 0.5 components. All the materials show a linear dependence on temperature, with the slopes and intercepts, however, strongly varying with composition. The behavior of the compound with a low doping level ($x = 0.1$) is similar to the undoped spinel $LiMn_2O_4$. As the amount

(45) Gao, Y.; Dahn, J. R. *J. Electrochem. Soc.* **1996**, *143*, 1783.
(46) Takada, T.; Akiba, E.; Izumi, F.; Chakoumakos, B. C. *J. Solid State Chem.* **1997**, *130*, 74.
(47) Tuller, H. L.; Nowick, A. S. *J. Phys. Chem. Solids* **1997**, *38*, 859.
(48) Goodenough, J. B.; Manthiram, A.; Wnetrzewski, B. *J. Power Sources* **1993**, *43*, 269.
(49) Masquelier, C.; Tabuchi, M.; Ado, K.; Kanno, R.; Kobayashi, Y.; Maki, Y.; Nakamura, O.; Goodenough, J. B. *J. Solid State Chem.* **1996**, *123*, 255.
(50) Sugiyama, J.; Hioki, T.; Noda, S.; Kontani, M. *J. Phys. Soc. Jpn.* **1997**, *66*, 1187.
(51) Greedan, J. E.; Raju, N. P.; Wills, A. S.; Morin, C.; Shaw, S. M.; Reimers, J. N. *Chem. Mater.* **1998**, *10*, 3058.
(52) Wallace, W. E. *Prog. Solid State Chem.* **1971**, *6*, 155.

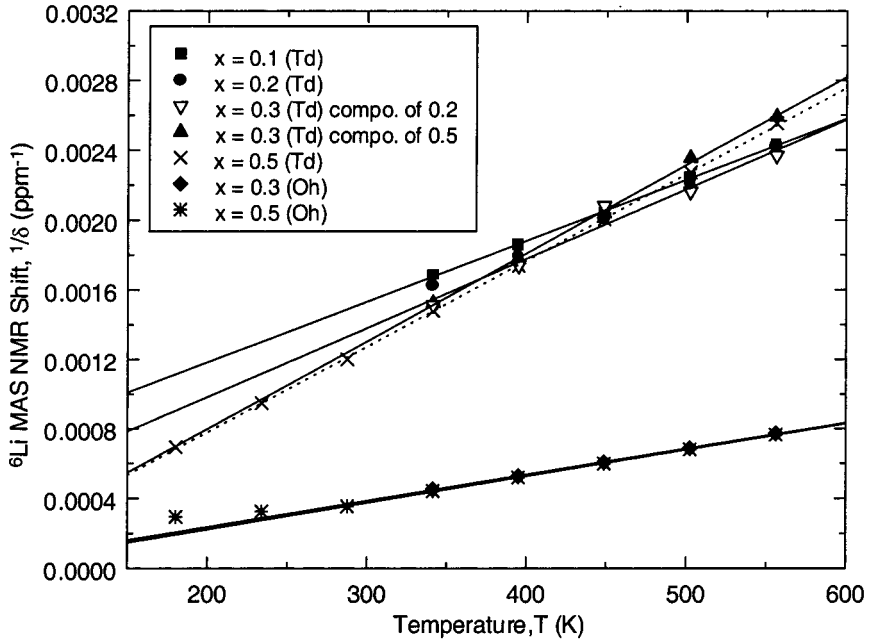


**Figure 10.** Plot of the inverse $^6$Li NMR shifts as a function of temperature. The temperature dependencies of the Li in the tetrahedral site and the octahedral site are shown separately on the plot for the $x = 0.3$ and 0.5 samples. An average shift for Li in the tetrahedral site of all the samples, determined from the center of mass of the resonances, was used. For the $x = 0.3$ sample, the analysis was performed for the two different components, i.e., $x = 0.2$ and 0.5. The solid lines (dashed lines for the tetrahedral sites of the $x = 0.5$ sample) represent the best fits to the experimental data.

of the Zn component increases, the values of the slopes and intercepts for $1/\delta = 0$ increase steadily; the value of $\theta$ is $-139$ K for $x = 0.1$, $-88$ K for $x = 0.2$, and 47 K (the average value of the intercepts derived for the tetrahedral and octahedral sites) for $x = 0.5$. The difference in the values of the Weiss constants for the $x = 0.2$ sample ($\theta = -88$ K) and the $x = 0.2$ component of the $x = 0.3$ sample ($\theta = -47$ K) is mainly due to the error associated with estimating the center of mass of the $x = 0.2$ resonances in the two-component mixture. These results are consistent with a progressive change from antiferromagnetic to ferromagnetic interactions with increased Zn-doping level.

**Electrochemical Studies of $LiZn_{0.1}Mn_{1.9}O_4$.** In contrast to the spinels doped with, for example, Cu and Ni, capacity is only seen at the 4 V region of the potential profile, since $Zn^{2+}$ is not oxidized. The 4 V region no longer contains two separate plateaus, which in $LiMn_2O_4$ is ascribed to lithium cation ordering in the 8a tetrahedral sites and two- or three-phase behavior.[53,54] Our previous $^6$Li NMR experiments of $LiMn_2O_4$, following charging, showed that this step in the voltage profile is associated with a significant change in the NMR shift: no change in the peak position (at approximately 520 ppm) was observed up to 50% charging, whereafter a second resonance was observed (at 640 ppm). The two resonances were observed to coexist from 50 to 80% charging (which corresponds to the two-phase region, as probed by in situ XRD).[55] In contrast, $LiZn_{0.1}Mn_{1.9}O_4$ shows a gradual change in the $^6$Li NMR spectra during charging, the resonance shifting gradually to higher frequency. This gradual increase in manganese oxidation state, as probed by the lithium ions remaining in the structure, is consistent with the gradual increase in potential as the charging proceeds. Furthermore, the lack of a discrete series of resonances is consistent with the suppression of the discontinuity in the potential profile curve, typically seen at around 50% charging in the stoichiometric materials. The disappearance of the series of resonances is ascribed to two different phenomena: (1) an increase in Li motion and (2) an increase in electron delocalization. In a study of $Li_{1.05}Mn_{1.95}O_4$, during charging, the fine structure returned (i.e., a series of discrete resonances were seen) when the temperature was lowered, consistent with both of these suggestions.[56] At a charging level of 70%, the main resonance (now at approximately 634 ppm) broadens considerably, suggesting a reduction in mobility. Similar behavior was observed in our previous charging experiment of the Ni-doped spinel.[29]

Previously, a resonance was observed at 830 ppm for $LiMn_2O_4$ synthesized at 650 °C at the end of charging and after multiple charging cycles, which was assigned to a defect spinel containing manganese ions with higher oxidation states.[55] Tarascon et al. proposed a series of possible defects that may be related to the oxidation−reduction peaks at 4.5 and 4.9 V: Mn ions in the tetrahedral sites, Li ions in the 16d octahedral sites, or oxidation of Mn to +5.[57] The X-ray refinement results of Li-excess spinels by Dahn et al.,[58] however, indicated that the cation mixing of Li and Mn in the 8a tetrahedral sites is not associated with the capacity at 4.5 V. The resonance due to the Li cations in the (16d)

(53) Liu, W.; Farrington, G. C.; Chaput, F.; Dunn, B. *J. Electrochem. Soc.* **1996**, *143*, 879.
(54) Gummow, R. J.; Thackeray, M. M. *J. Electrochem. Soc.* **1994**, *141*, 1178.
(55) Lee, Y. J.; Wang, F.; Mukerjee, S.; McBreen, J.; Grey, C. P. *J. Electrochem. Soc.* **2000**, *147*, 803.
(56) Lee, Y. J.; Eng, C.; Grey, C. P. *Electrochem. Soc. Symp. Proc.* **2001**, *148*, A249.
(57) Tarascon, J. M.; Mckinnon, W. R.; Coowar, F.; Bowmer, T. N.; Amatucci, G.; Guyomard, D. *J. Electrochem. Soc.* **1994**, *141*, 1421.
(58) Gao, Y.; Dahn, J. R. *J. Electrochem. Soc.* **1996**, *143*, 100.

octahedral sites was observed for $LiZn_{0.1}Mn_{1.9}O_4$ even at the end of charging, indicating that the 16d Li are not removed at <4.5 V. (N.b., given the signal-to-noise associated with the spectrum, it is difficult to determine whether a small fraction of the 16d Li sites is removed.) Thus, we assign the resonance at 822 ppm, observed close to the end of charge, to environments such as $Li(OLi)(OMn^{4+})_{11}$, which is reasonable based on the hyperfine shift of the tetrahedral Li ions in the $x = 0.5$ compound. Interestingly, this also suggests that this environment is present in $LiMn_2O_4$ synthesized at lower temperatures, following deintercalation.

The resonance at 643 ppm must be due to Li ions near residual $Mn^{3.5+}$ ions that are still not deintercalated, even at 4.5 V. The presence of residual lithium sites is consistent with an initial capacity of ~80 mAh $g^{-1}$ for this material, which is significantly lower than the calculated theoretical capacity (118 mAh $g^{-1}$, based on a final composition $Li_{0.2}Zn_{0.1}Mn_{1.9}O_4$). In our previous work, the Ni-doped spinel prepared under the same conditions showed a higher capacity at the 4 V region (101 mAh $g^{-1}$). Lower initial capacities have, however, been observed by other workers for the Mg- and Zn-substituted spinels (85 mAh $g^{-1}$ for $LiMg_{0.1}Mn_{1.9}O_4$ and 100 mAh $g^{-1}$ for $LiZn_{0.05}Mn_{1.95}O_4$).[7] There are a number of possible explanations for this including (i) Li cation vacancies; this is consistent with the neutron diffraction results for the $x = 0.5$ compound and (ii) blockage of the lithium-ion diffusion pathways. The presence of the resonance at 643 ppm suggests that there are Li sites near $Mn^{3+}$ ions that are still not deintercalated, due to kinetic factors that appear to prevent lithium-ion deintercalation at a charge rate of C/8. The lithium cations in these spinel compounds migrate in three dimensions via empty neighboring 16c octahedra, which share the common faces with 8a tetrahedral sites. The substituted $Zn^{2+}$ cations partially occupy the 8a tetrahedral sites and may restrict the diffusion pathway for the $Li^+$ ions. The decreased capacity of the Zn-doped spinel is presumably due to a combination of both effects.

## Conclusions

Li NMR has been shown to be a sensitive probe of the local coordination environments for Li in Zn-doped lithium manganese oxides. Two crystallographically inequivalent sites are observed for all the doping levels, i.e., Li in the tetrahedral and octahedral sites. This indicates that Zn cations replace the Li in the tetrahedral sites, resulting in an inverse spinel. $Zn^{2+}$ substitution increases the oxidation state of nearby Mn, resulting in a series of Li NMR resonances with larger shifts than the shift of the normal spinel when the extent of Zn substitution is low. These resonances are assigned to Li ions with different numbers of $Mn^{3+}$ and $Mn^{4+}$ ions in their local coordination sphere. This should be contrasted to the stoichiometric material $LiMn_2O_4$ where the electrons in the $e_g$ orbitals are delocalized over the whole sample, as expected for a hopping semiconductor. Analysis of the intensities and hyperfine shifts of the additional resonances in $LiZn_{0.1}Mn_{1.9}O_4$ indicates that the $Mn^{4+}$ ions (or electron holes) are localized near octahedral $Li^+$ and not randomly distributed in the lattice. No resonances due to environments such as $Li(OMn^{3.5+})_{11}(OLi)$ were seen, confirming that the manganese ions near $Li^+$ in the octahedral sites are oxidized to $Mn^{4+}$; these local environments may also be preferentially occupied by Zn. The series of resonances collapse into the main resonance at high temperature, which is ascribed to a combination of electron-hole delocalization and lithium-ion motion.

For the sample with $x = 0.5$, a superstructure characteristic of Li/Zn and Mn/Li ordering in the tetrahedral and octahedral sites, respectively, is observed by XRD and NPD, consistent with the narrow $^6Li$ resonances observed by MAS NMR. In contrast, the material with no cation ordering, obtained by quenching from high temperature, shows a very broad $^6Li$ NMR resonance due a distribution of local environments for Li. At a doping level of $x = 0.3$, a two-phase mixture (with compositions $x = 0.5$ and 0.2) is formed instead of a single-phase solid solution. The phase instability is ascribed to the additional Madelung energy that can be achieved by cation ordering on the tetrahedral and octahedral sites, for the $x = 0.5$ level, vs the additional entropy associated with disorder. NMR was used to probe the magnetic correlations between the electron spins and showed a gradual change in the nature of the interactions between Mn ions from antiferromagnetic at low doping levels to ferromagnetic when $x = 0.5$.

The electrochemical study of $LiZn_{0.1}Mn_{1.9}O_4$ showed a gradual shift in the $^6Li$ peak position to higher frequency, which is ascribed to a gradual increase in the average manganese oxidation state, as probed by Li. This is consistent with the gradual increase in potential, as charging proceeds. The series of resonances collapse during charging due to lithium ion/electron mobility. We tentatively suggest that the presence of $Li^+$ ions in the 16d sites of the three-dimensional tunnel structure results in a distribution of Li local environments, which helps to prevent the formation of a series of phases containing long-range Li ordering during charging and improves the lithium mobility of a subset of the ions, accounting for the good capacity retention of the material. The poorer initial capacity is ascribed to Li ions that are stuck in the lattice due to the presence of $Zn^{2+}$ ions or to the presence of Li in local environments such as $Li(OLi)(OMn^{4+})_{11}$, which do not contain $Mn^{3+}$ ions in their local environments and are therefore not readily oxidized at 4 V.

**Acknowledgment.** This work was supported by the National Science Foundation (DMR-9901308 and -0095633). C.E. thanks the Arnold and Mabel Beckman Foundation for the Beckman Scholars Award. The research carried out at the NSLS at BNL is supported under Contract No. DE-FG02-86ER45231 with the U.S. Department of Energy, BES. We acknowledge the support of the National Institute of Standards and Technology, U.S. Department of Commerce, in providing the neutron research facilities used in this work and Brian Toby for help with the data collection.

CM010503J